Carbon 146 (2019) 528–534

Contents lists available at ScienceDirect

Carbon

journal homepage: www.elsevier.com/locate/carbon

Insights into dynamic molecular intercalation mechanism for Al–C battery by operando synchrotron X-ray techniques

Di-Yan Wang [a, *], Shao-Ku Huang [b], Hsiang-Ju Liao [a], Yu-Mei Chen [a], Sheng-Wen Wang [a], Yu-Ting Kao [a], Ji-Yao An [a], Yi-Cheng Lee [a], Cheng-Hao Chuang [c], Yu-Cheng Huang [c], Ying-Rui Lu [d], Hong-Ji Lin [d], Hung-Lung Chou [e], Chun-Wei Chen [b], Ying-Huang Lai [a, **], Chung-Li Dong [c, ***]

[a] Department of Chemistry, Tunghai University, Taichung, 40704, Taiwan
[b] Department of Materials Science and Engineering, National Taiwan University, Taipei, 10617, Taiwan
[c] Department of Physics, Tamkang University, Tamsui, 25137, Taiwan
[d] National Synchrotron Radiation Research Center, Hsinchu, 30076, Taiwan
[e] Graduate Institute of Applied Science and Technology, National Taiwan University of Science and Technology, Taipei, 10607, Taiwan

ARTICLE INFO

Article history:
Received 15 November 2018
Received in revised form
2 January 2019
Accepted 11 January 2019
Available online 18 February 2019

Keywords:
Al ion battery
X-ray absorption spectroscopy
In-situ X-ray diffraction
Simulated core-level spectrum
Anion intercalation

ABSTRACT

Recently, a novel rechargeable Al ion battery (AIB) with high performance has been developed. Owing to its low cost, high-rate capability, excellent cyclability, and non-flammability, AIB provides a safe alternative to many commercial batteries used in the energy storage system. To improve its performance, identifying molecular structure and arrangement of chloroaluminate anion ($AlCl_4^-$) intercalated in the graphite layer remains a great challenge. In this work, operando analysis of X-ray diffraction (XRD) measurement and X-ray absorption (XAS) spectroscopy were performed to investigate the intercalation of $AlCl_4^-$ anion and related molecular arrangement in the graphite layers. The intercalated stage and intercalant gallery height of graphite cathode electrode during AIB battery operation were observed to be stage 3 and 9.22 Å, respectively. Furthermore, the spectral evolution from ex-situ XAS at the Al and Cl K-edge was associated with closely packed intercalation of $AlCl_4^-$ molecules. With density functional theory (DFT) calculation, three simulated models of intercalated $AlCl_4^-$ molecules in the graphite layer were revealed successfully, which explained possible molecular structures at different charging states. This analytical methodology paves the way for better understanding the structural transformation of molecular ions de-/intercalation in graphite layers.

© 2019 Elsevier Ltd. All rights reserved.

1. Introduction

Rechargeable batteries have been viewed as essential parts in the energy storage system [1,2]. To aspire the higher energy density than traditional lithium ion battery used wildly, the rechargeable Al-based battery has been considered as a breakthrough battery technology because an Al^{3+}/Al redox couple demonstrated highly competitive gravimetric capacity and volumetric capacity relative to single-electron Li^+/Li or Na^+/Na redox reactions during the electrochemical redox reaction [3]. Recently, several reports indicated that a high-performance rechargeable aluminum ion battery with high-rate capability was successfully developed by using an Al anode and different graphitic materials cathode (so-called Al–C battery) such as pyrolytic graphite [4], 3D graphite foam [4,5], carbon paper [6], expanded graphite [7] graphene paper [8,9] and highly crystallinity graphite powder [10–12], etc. The workable Al–C battery is attributed to right choice of the ionic electrolyte made by mixing 1-ethyl-3-methylimidazolium chloride ([EMIm]Cl) with aluminum chloride ($AlCl_3$) to form chloroaluminate anions ($AlCl_4^-$ and $Al_2Cl_7^-$). The anode reaction of Al–C battery has been discovered to exhibit good reversible electrochemical deposition and dissolution of aluminum in the ionic liquid (IL) electrolyte with appropriate ratio of [EMIm]Cl and $AlCl_3$ [13–17]. The cathode reaction of Al–C battery was supposed to the intercalation and

* Corresponding author.
** Corresponding author.
*** Corresponding author.
E-mail addresses: diyanwang@thu.edu.tw (D.-Y. Wang), yhlai@go.thu.edu.tw (Y.-H. Lai), cldong@mail.tku.edu.tw (C.-L. Dong).

https://doi.org/10.1016/j.carbon.2019.01.038
0008-6223/© 2019 Elsevier Ltd. All rights reserved.

deintercalation of $AlCl_4^-$ anions during charging and discharging reaction [4]. However, the detailed intercalation mechanism of anions was still unclear. Therefore, developing a powerfully analytical technique to realize the molecular structure and arrangement of chloroaluminate anion ($AlCl_4^-$) intercalated in the graphite layer remains a key issue for further improving the performance of rechargeable Al–C battery.

The theoretical calculation has been considered as a good approach to understand the information of metal ions or molecular structure (Rüdorff [18] and Daumas–Hérold models [19]) when they were intercalated in the graphite layers [20,21]. By utilizing calculation method, valuable information including intercalated stage, intercalant gallery height [22,23], formation energy of graphite intercalation compound (GIC) [24–26], intercalation voltage [23] and even supposed intercalant structure [27,28] can be obtained. For example, GICs with $AlCl_4^-$ intercalated was calculated to be favored at stage 3 with lower formation energy by using first-principles calculations. The stage 3 of GIC means that three graphite layers with no guest material in between alternate with an intercalated layer. A model of doubly stacked $AlCl_4^-$ layers in the graphite layer at stage 3 was also constructed to find that the anion conductivity was increased with the reduced film thickness. It could be attributed to high elasticity of few-layered graphene, providing more space for facile $AlCl_4^-$ diffusion [22]. In addition, based on the DFT calculation, some reports suggested that a planar structure of $AlCl_4^-$ ions was formed when anions were intercalated between graphite layers, resulting in high rate performance of ion diffusion through the graphite cathode [27]. However, without the direct evidence from analytic spectroscopy, it is difficult to build an accurate simulation model. X-ray absorption spectroscopy (XAS) is an elemental-selective and chemical-sensitive approach and has been considered as a powerful technique for characterization of the local geometric structure and electronic structure of complex materials [29]. In XAS analysis, the absorption feature originated from core electron (K-, L-, and M-edges) excited by incident X-rays determines the density of unoccupied electronic states [30]. When the molecular structure is modulated under different stimuli, the interaction between atoms varies, affecting the density of electronic states, and thus resulting in different x-ray absorption spectral profiles. Therefore, when $AlCl_4^-$ anion is intercalated in the graphitic layers under the recharging process, the studies of the Al and Cl K-edge XAS data will be great helpful to investigate the structure changes or arrangement of the anions in the graphite layers.

In this work, operando XRD measurement and XAS analysis of Al, Cl and C K-edge of natural graphite (NG) electrode in Al–C battery were carried out under different charging and discharging states. The intercalant stage and gallery height were derived from the in-situ XRD data. Based on this result, the related intercalating structure arrangement models of $AlCl_4^-$ anions were constructed by using DFT calculation. The intercalated molecular structure of $AlCl_4^-$ anion in the graphite layer under different charging states are revealed successfully by coupled ex situ XAS and simulated core-level spectra.

2. Experimental Section

2.1. Preparation of freestanding natural graphite flake (NG) electrode

The fabrication method was modified by our previous work [10]. First, the graphite flake slurry was formed by a mixture of SP-1 graphite powder (TED PELLA, Inc. Prod. No. 61–302, Lot# 042111) and polyvinylidene difluoride (PVDF) (10%) (HSV-900) in N-methyl pyrrolidinone (NMP, Alfa Aesar, 99+%). Then, the slurry was cast on a Cu foil (Ubiq Tech. Inc. LTD, 10 μm) to form a uniform graphite film and dried at 150 °C for 2 h. The Cu foil was then etched by iron chloride ($FeCl_3$, Sigma-Aldrich, 97%) solution (0.4 g/mL) to form a freestanding NG film. After the NG film was rinsed with deionized water and wait for dried at 70 °C for 3 h to obtain the NG film (1 cm × 1 cm). The specific graphite loading was ~4 mg cm^{-2}.

2.2. Preparation of [EMIm]Al_xCl_y ionic liquid electrolytes

An ionic liquid electrolyte was prepared by a mixture of 1-ethyl-3-methylimidazolium chloride ([EMIm]Cl, IolitecIL0093-HP-0100, >98%) and anhydrous aluminium chloride ($AlCl_3$, Alfa Aesar, 99%) with a mole ratio of 1–1.3 in a glove box under Argon gas.

2.3. Electrochemical characterization

In galvanostatic test, the upper and lower cut-off potentials were set at 2.5 and 0.5 V vs. Al respectively with SP-50 Potentiostat from BioLogic ltd with a constant current of 100 mA/g.

2.4. In-situ X-ray diffraction measurement

The *in-situ* XRD measurement was taken with NG/Al pouch cell under charging and discharging at a constant current density of 100 mAg^{-1} with the cut-off voltage of 0.5 and 2.45 V vs. Al. The pouch was opened windows with an area of 0.25 cm^2 in the center of two sides of pouch cell. The windows of pouch cell were covered with Kapton tape to prevent electrolyte from contacting with air. *In-situ* XRD analysis were performed at the beamline of BL23A small/wide angle X-ray scattering (SWAXS) at Taiwan Light Source (TLS) and the beamline of 09A at the Taiwan Photon Source (TPS) in National Synchrotron Radiation Research Center (NSRRC). The 15 keV (wavelength $\lambda = 0.827$ Å) X-ray sources are delivered from the superconducting wavelength-shifting magnet and a Si(111) double-crystal monochromator, respectively [31,32]. With a rapid position-sensitive detector (Mythen 24K or Mythen 3K), *in-situ* XRD patterns were collected at 0.5 or 2 frames per min. Diffraction angle θ was calibrated with Si powders (NBS640b) and silver behenate. One-dimensional XRD profiles were integrated from selected fan-like areas of the symmetrical 2D powder rings using the Fit2D program [33]. Crystal structure parameters were refined with the Rietveld method[5] using the GSAS program and the angle calibration was performed according to LaB_6 (SRM 660c) and/or Si powders (NBS640b) standard. With software transformation, the representation of in-situ XRD spectra with 2θ as x-axis is based on the wavelength of 1.5406 Å.

2.5. Ex-situ X-ray absorption measurement

The XAS were conducted at Taiwan Light Source (TLS) with electron beam energy 1.5 GeV and with ring current 360 mA top-up operation, at National Synchrotron Radiation Research Center (NSRRC), Hsinchu, Taiwan. The Al K-edge was carried out with fluorescence yield mode recorded by 7-element detector at soft x-ray beamline BL11A1, which is a Dragon type (spherical grating monochromater (SGM)) beamline equipped with separate horizontal and vertical focusing mirrors, and a movable slit. Al foil is used for energy calibration of Al K-edge. The resolving power (E/delta E) is about 10000 and the base pressure of the measurement is about 2×10^{-9} torr. The Cl K-edge was obtained by recording fluorescence yield with using an ionization chamber at tender x-ray beamline BL16A1, which is equipped with double crystal (Si (1110)) monochromater (DCM). Ru L3-edge (2838 eV) of a Ru foil is used for energy calibration of Cl K-edge (2822 eV) and the resolving power (E/delta E) is about 7000. The beam size of both Cl K- and Al K-edge

measurements were about 2 mm × 2 mm. To prevent behavior change of anion intercalated in the graphite layers, the ionic liquid electrolyte was only eliminated by kimwipes without washed by solvent.

2.6. Theoretical calculations

The first-principles calculation was performed based on the density functional theory in the CASTEP code [34]. The on-the-fly generation of ultrasoft pseudopotential and the Perdew-Burke-Ernzerhof generalized gradient approximation were also used [35,36]. The energy cutoff was set as 350 eV and used for plane waves. Electronic structure was optimized until the force on each atom was smaller than 0.03 eV $Å^{-1}$. A 4 × 4 X 2 k-point mesh was used for Brillouin-zone integrations. Due to the Van der Waals interactions, the DFT-D approach was used for the correction in the GICs. The simulation of XRD pattern was obtained by using the Powder Diffraction function in Reflex module included in software Materials studio.

3. Results and discussion

3.1. Intercalation analysis of $AlCl_4^-$ anion by in-situ XRD measurement

To investigate the intercalating behavior of $AlCl_4^-$ anions in the graphite layer with different charging and discharging voltages, in-situ XRD measurement during battery operation were performed as shown in Fig. 1. The corresponding charging and discharging state of NG/Al battery in each XRD pattern (Fig. 1 (a), left part) is consistent with the galvanostatic curve which possesses the specific capacity of 95 mAh/g (Fig. 1 (a), right part). Initially, the (002) diffraction peak of graphite is found at 2θ~26.50°. Fig. 1 (b) showed that the selected XRD pattern of NG/Al battery at pristine, fully-charged and fully-discharged status. When the battery was charged to 2.45 V, the peak of 26.50° disappeared along with the appearance of dominant peaks including 5.52°, 11.1°, 16.82°, 22.59° and 28.19°, which can be assigned to (001), (002), (003), (004) and (005), respectively. These phases are in good agreement with the previously literature reports [10,37]. During the discharging process, the splitting peak can recover to origin (002) peak (26.50°) of graphite, meaning that graphite can be recovered during anion intercalation and deintercalation process.

Especially, under fully charged state, the intensity of (005) peak at 28.2° is higher than that of (004) at 22.5° and the intensity ratio of (005)/(004) is around 1.5 fold which is quite different from the results of metal ion or other anion intercalated in the graphite layers [38–40]. The different intensity of peak in XRD patterns could be ascribed to be structure arrangement of molecules in the graphite layer. The detailed calculation of intercalant gallery height of $AlCl_4^-$ in the graphite was described in the supporting information. In order to determine the stage number of fully charged status, the value ~1.25 of $d_{(004)}/d_{(005)}$ was calculated [38]. From the stage calculated in graphite intercalated compound [41,42], our NG cathode achieved stage 3 when the battery is fully charged to 2.45 V. The results can determine the intercalant gallery height (d_i), the relationship between unit cell repeat distance (I_c), intercalant gallery height (d_i), stage number (n) and observed distance (d_{00l}) was obtained as Equation (1) [21].

$$I_c = d_i + (n-1) \times 3.35Å = l \times d_{00l} \quad (1)$$

By putting d_{001} value into Equation (1), the intercalant gallery height (d_i) and unit cell repeat distance (I_c) equal to 9.22 Å and 15.92 Å.

3.2. X-ray absorption spectra of Al and Cl K-edge for Al–C battery

To further investigate the structural information and the chemical modifications of graphite cathode electrode upon the charge-discharge process, XAS at the Al and Cl K-edge and related core-level simulation were performed, as shown in Fig. 2. The Al K-edge spectra (Fig. 2a) shows that the observed spectral profiles of graphite electrode vary as a function of different charged and discharged states, which demonstrates different amounts of $AlCl_4^-$ intercalated in the electrode. There are two peaks (A and B peaks) found in Al K edge spectra, which are located at 1568 eV and 1571 eV, respectively. It is expected that the unoccupied electronic states exhibit significant differences under different structural geometries and ligand environments [43]. The main peak (A) represents the tetrahedral coordinated Al; interaction between Al s orbital of adjacent $AlCl_4^-$ anions (see supporting information). Notably, the Al 3p orbitals participate in chemical bonding directly. Therefore, the second absorption peak (B) is attributed to the interaction between Al 3p orbitals of Al atoms of adjacent $AlCl_4^-$ anions (see supporting information). According to the analytical

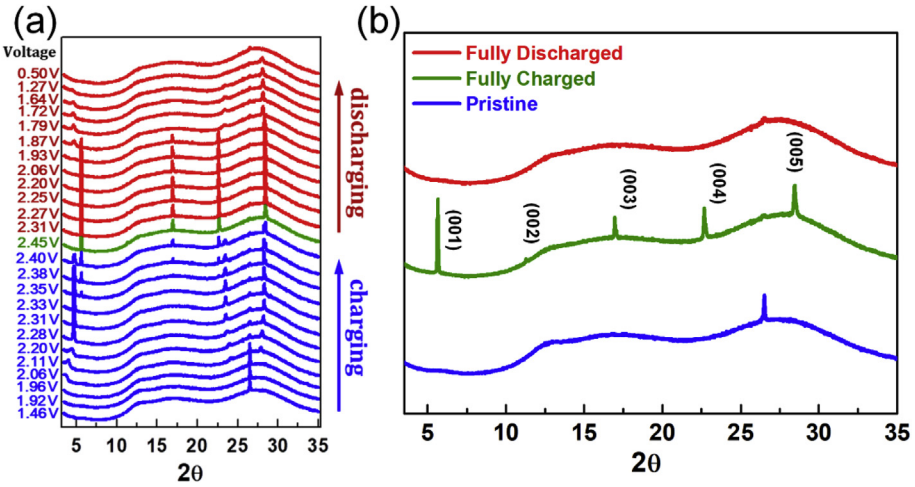

Fig. 1. (a) The In situ XRD patterns of NG/Al battery collected during second cycle at 100 mA/cm^2 which charging and discharging curve is shown at the right. (b) The selected XRD pattern of NG/Al battery at pristine, fully-charged and fully-discharged status. (A colour version of this figure can be viewed online.)

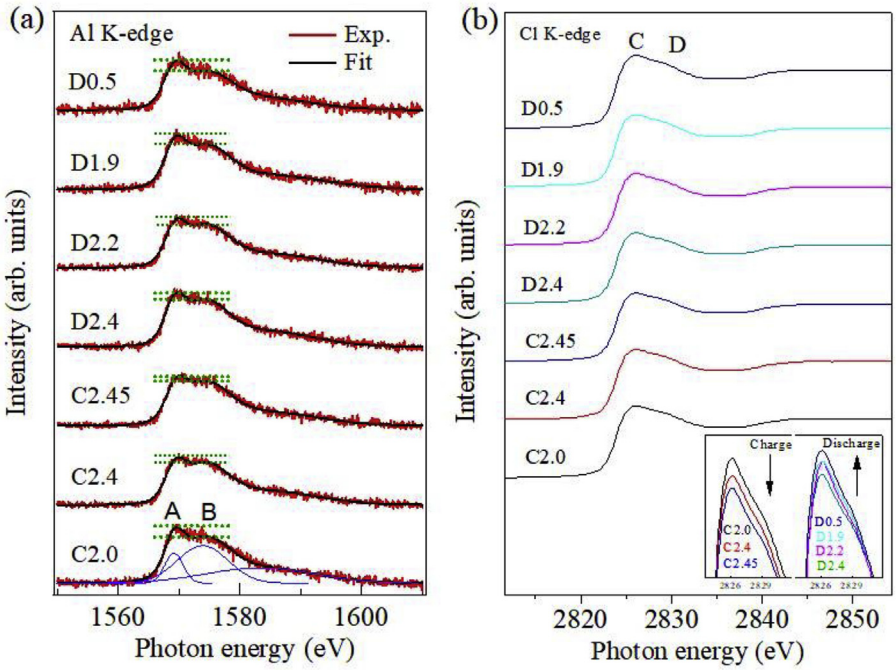

Fig. 2. *Ex-situ* X-ray absorption spectra at the (a) Al K-edge and (b) Cl K-edge of natural graphite in various charging and discharging states (denoted as C and D, respectively) through the second cycle. Two distinguished peaks A and B in Al K-edge spectra and peaks C and D in Cl K-edge spectra. (A colour version of this figure can be viewed online.)

curve-fitted data (the bottom of Fig. 2a), differences in the intensities of peak A and B are clearly observed after the background subtraction. Fig. 2 (b) displays XAS Cl K-edge of the graphite electrode with the various charged/discharged states. All the spectra exhibit similar profiles with a main absorption feature at 2826 eV (C peak) and a high energy peak at 2829.6 eV (D peak), but the intensity varies upon charging/discharging, as seen in the right-bottom inset of Fig. 2 (b). The change of the intensity ratio (peak A/peak B) in Al K-edge and the revolution of C and D peaks in Cl–K edge were believed to be related to the different structural arrangement of $AlCl_4^-$ anion intercalated in the graphite electrodes.

3.3. X-ray absorption spectra of C K-edge for Al–C battery

The intercalation of $AlCl_4^-$ in between Cl and carbon of graphite were also investigated by the C K-edge XAS, as displayed in Fig. 3. It is well known that there are generally two characteristic peaks appeared at 284 eV and 290.2 eV that associate with π^* (sp^2) and σ^* (sp^3) states, respectively, in carbon-based materials. Two extra peaks observed in-between are originated from C–H and/or C–N bonding (285.8 eV) and C–Cl bonding (287.3 eV) [10,44]. The appearance of peak F is a direct indication of forming C–Cl bonding as the $AlCl_4^-$ is intercalated. The intensity of such a peak varies for various charged/discharged states. In our previous work, we suggested that one possibility is the formation of C–Cl bonding on the surface or edges of NG flakes [10]. To further glean more insight, we found that the C2.0 spectrum has the most intense π^* peak reflecting stronger sp^2-hybridized states. In the charged electrode, the intensity of π^* peak decreases significantly. Then, the intensity of this peak is restored upon the de-/intercalation of $AlCl_4^-$. In order to clarify this aspect, the area of peak E and peak F for different charged and discharged states of electrodes are integrated after the background subtraction, and is displayed in the inset of Fig. 3. Notably, as the $AlCl_4^-$ is intercalated (de-/intercalated) between the graphite layer, the intensity of peak F is increased (decreased)

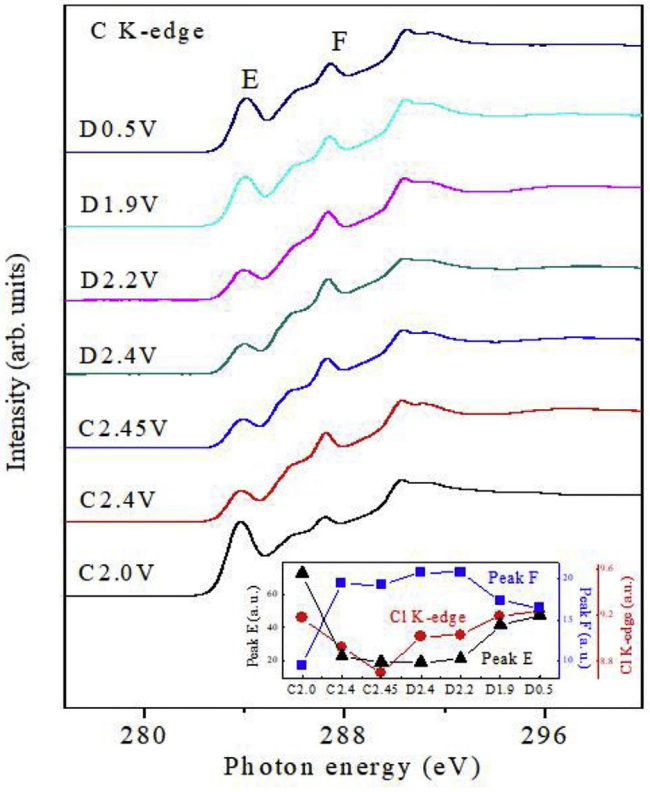

Fig. 3. *Ex-situ* X-ray absorption spectra at the C K-edge of natural graphite in various charging and discharging (denoted as C and D, respectively) through the second cycle. Inset shows the evolution of peak E and F at different charged and discharged states of electrodes. (A colour version of this figure can be viewed online.)

which directly infers the chemical bond formed between Cl and C. It is noted that the intensity variation of Cl K-edge is decreased (increased) as the $AlCl_4^-$ is embedded (extracted) which exhibit the opposite trend to peak F, implying there could be a charge transfer between Cl and C, because the electronegativity of Cl and C are 3.16 and 2.55, respectively. Thus, as more and more $AlCl_4^-$ anions are intercalated, more charge transfer from C to Cl are obtained, leading to increased (decreased) intensity of peak F in C K-edge (Cl K-edge). The same trend between Cl K-edge and peak E is found and this could be owing to the covalent character of C sp^2-Cl 3p states. In addition, the intercalant gallery height is enlarged by embedded $AlCl_4^-$ and this would modify the morphology of graphite layer and thus affect the sp^2 hybridized orbitals, resulting in decrease of the π-π stacking interaction and degradation of the C sp^2 states.

3.4. The proper DFT simulation models of $AlCl_4^-$ anion

To construct the geometry of GICs with $AlCl_4^-$ anion intercalated, DFT calculation [34] was utilized according to the intercalant gallery height (9.22 Å) and intercalated extent of stage 3 found in the in-situ XRD measurement. Fig. 4 a-c shows that three proper models, including X-shape loosed model, X-shape packed model and upside-down model were constructed by three layers of 54 carbon atom with one or two $AlCl_4^-$ for different intercalation conditions with 3×3 repetition of the graphite primitive unit cell. These models were collected from the simulated XRD patterns which can compared to in-situ XRD results (see supporting information). For two X-shape models (Fig. 4a and b), $AlCl_4^-$ showed tetrahedron structure lying with two Cl atoms pointing up and the other two down. The distances between two $AlCl_4^-$ anions for X-

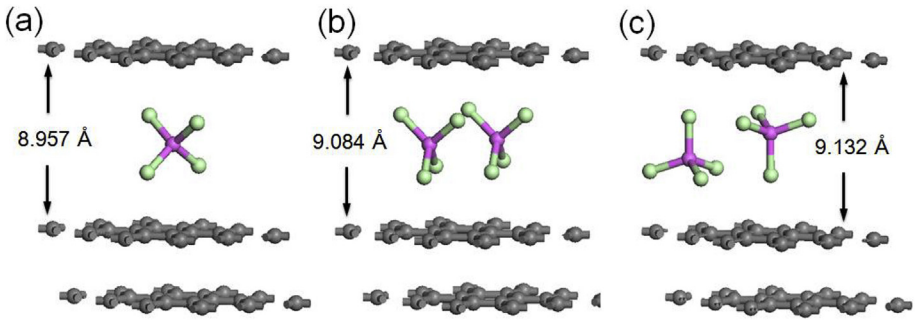

Fig. 4. Optimized structures of (a) X-shape loosed model, (b) X-shape packed model and (c) upside-down model includes one or two $AlCl_4^-$ anions intercalation in the graphite layer which are constructed by 3×3 repetition of the graphite primitive unit cell. Three plausible simulation models were evidenced from simulation XRD patterns of stage-3 (in Fig. S3). (A colour version of this figure can be viewed online.)

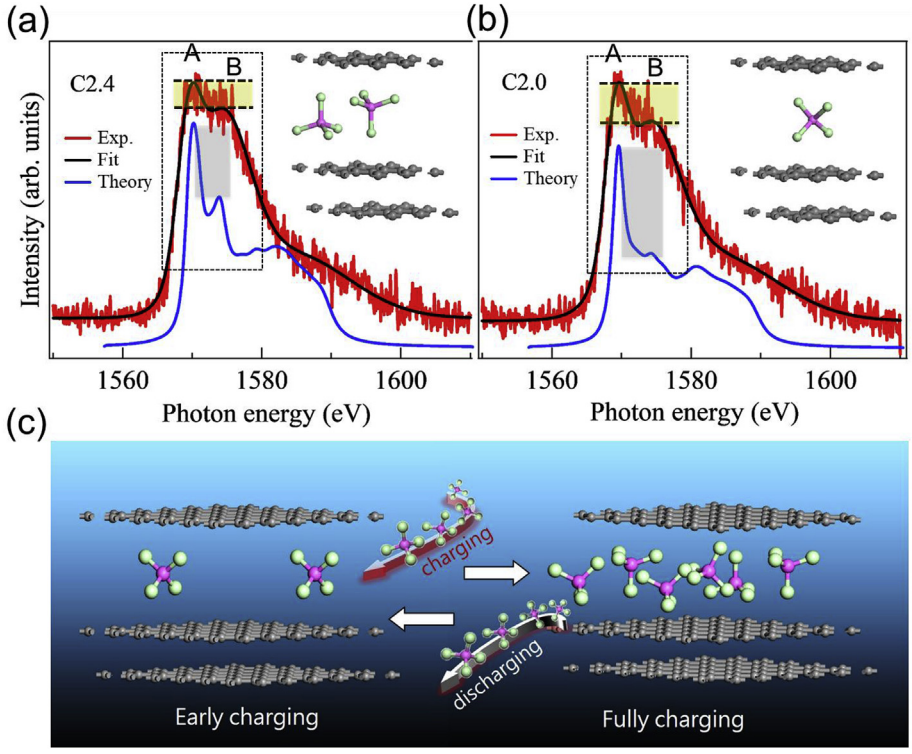

Fig. 5. The corresponding core-level simulation spectra (Al K edge) of (a) the upside-down model and (b) X-shape loosed model were compared with different charging states. (c) Schematic illustration of the structural arrangement of $AlCl_4^-$ anion intercalating in the graphite layer under early, fully charging and discharging states. (A colour version of this figure can be viewed online.)

shape loosed and packed models are 12.011 Å and 5.519 Å, respectively. In the upside-down model, the two $AlCl_4^-$ molecules with a distance of 4.496 Å showed that one is standing with one Cl atom and other is standing with three Cl atoms along with graphite layers.

To investigate the evolution of absorption peaks (A and B) for Al K-edge in XAS spectra under different charging and discharging states, the theoretical core level spectra [35] of Al K edge were obtained and demonstrate the different geometries of intercalated $AlCl_4^-$ based on the representative upside down model and X-shape loosed model, as shown in Fig. 5 (a) and 5 (b), respectively. In comparison with the deconvoluted spectra of the samples charging at 2.4 V and 2.0 V, the peak B is enhanced at high charging state and then declined during discharging which is consistent with that of upside down model and X-shape loosed model, respectively. Also, there is a similar result for core-level simulation spectra of X-shape packed model in comparison with that of upside down model (see supporting information). The results suggested that as the $AlCl_4^-$ was initially intercalated into the graphite layer, the complex was in tetrahedral arrangement with two Cl pointing up and two other pointing down, or closed packed X shape structure. Differences in the symmetry of $AlCl_4^-$ arrangement are expected to reflect changes in the local electron density environment around the Al atom, and the differences in the peak ratio suggest change in the unoccupied orbital, indicating changes in Al bonding to ligands. According to XAS and core-level simulation results, the structural arrangement of $AlCl_4^-$ anion intercalating in the graphite layer under early and fully charging states can be revealed clearly, as shown in Fig. 5 (c). As more and more $AlCl_4^-$ was embedded in the graphite layer, they tended to form closed packed $AlCl_4^-$ complexes. On the contrary, during discharging process, the closed packed $AlCl_4^-$ complexes will be deintercalated from the graphite layer into the electrolyte and structure arrangement will recover to loosed behavior gradually. Several simulation reports have provided different possible molecular models to discuss the formation energy of different intercalant stages or molecular structure of $AlCl_4^-$ intercalating in the graphite layer [22,23]. However, due to lack of experimental evidences from spectroscopic analysis, the accuracy of simulation models will be questioned. Therefore, helped by the operando analysis of synchrotron XAS and XRD, the various models of $AlCl_4^-$ molecular structures in the graphite layer at different charging and discharging states were successful constructed more accurately. It's believed that the established analytical methodology will provide a good route for better understanding the structural transformation of molecular ions de-/intercalation in graphite layers.

4. Conclusions

The molecular arrangement structure of $AlCl_4^-$ intercalating into graphite layers under different charging and discharging states has been revealed by X-ray spectroscopic technique and core level spectra of DFT simulation. It was found that the variation of XAS spectral profile strongly depended on the molecular arrangement structure of chloroaluminate, manifested by simulated spectra of DFT core-level calculation. At the fully charged state, the structural arrangement of $AlCl_4^-$ molecules exhibited a mixing of X-shape packed model or upside-down model. Analytical results provide deeper insights into molecular structure of intercalants in the graphite layer. These findings suggested that our approaches can be extended to investigate other intercalating molecular structure of anion or cation molecules in graphite layers for developing next-generation batteries.

Conflicts of interest

None.

Author contributions

D-Y Wang, Y-H Lai, and C-L Dong conceived the project and designed the experiments. D Wang, H-J Liao, Y-T Kao, J-Y An and Y-C Lee performed material preparation, structural characterization, and electrochemical measurements. Y-M Chen, S-W Wang, Y-H Lai and D-Y Wang perform the in-situ X-ray XRD measurement. C-H Chuang, Y-C Huang, Y-R Lu, H-J Lin, perform the X-ray absorption measurements. S-K Huang, H-L. Chou, and C.W. Chen perform the DFT and First Principle Calculation. D. Wang, S-K Huang and C-L Dong analyzed the data. D. Wang and C-L Dong co-wrote the paper. All authors discussed the results and commented on the manuscript.

Acknowledgements

This work has been financially supported by Ministry of Science and Technology, Taiwan (MOST 106-2113-M-029-006-MY2 and MOST 106-2632-M-029-001) and Tunghai University. We thank Dr. U-Ser Jeng for assistance at beamline BL23A at Taiwan Light Source (TLS) and Dr. Hwo-Shuenn Sheu, Dr. Yu-Chun Chuang for assistance at beamline 09A at the Taiwan Photon Source (TPS).

Appendix A. Supplementary data

Supplementary data to this article can be found online at https://doi.org/10.1016/j.carbon.2019.01.038.

References

[1] D. Larcher, J.-M. Tarascon, Towards greener and more sustainable batteries for electrical energy storage, Nat. Chem. 7 (1) (2015) 19–29.
[2] B. Dunn, H. Kamath, J.-M. Tarascon, Electrical energy storage for the grid: a battery of choices, Science 334 (6058) (2011) 928–935.
[3] Q. Li, N.J. Bjerrum, Aluminum as anode for energy storage and conversion: a review, J. Power Sources 110 (1) (2002) 1–10.
[4] M.-C. Lin, M. Gong, B. Lu, Y. Wu, D.-Y. Wang, M. Guan, M. Angell, C. Chen, J. Yang, B.-J. Hwang, H. Dai, An ultrafast rechargeable aluminium-ion battery, Nature 520 (7547) (2015) 324–328.
[5] X. Yu, B. Wang, D. Gong, Z. Xu, B. Lu, Graphene nanoribbons on highly porous 3D graphene for high-capacity and ultrastable Al-ion batteries, Adv. Mater. 29 (4) (2017) 1604118.
[6] S. Jiao, H. Lei, J. Tu, J. Zhu, J. Wang, X. Mao, An industrialized prototype of the rechargeable Al/AlCl 3-[EMIm] Cl/graphite battery and recycling of the graphitic cathode into graphene, Carbon 109 (2016) 276–281.
[7] Y. Wu, M. Gong, M.C. Lin, C. Yuan, M. Angell, L. Huang, D.Y. Wang, X. Zhang, J. Yang, B.J. Hwang, H. Dai, 3D graphitic foams derived from chloroaluminate anion intercalation for ultrafast aluminum-ion battery, Adv. Mater. 28 (41) (2016) 9218–9222.
[8] L. Zhang, L. Chen, H. Luo, X. Zhou, Z. Liu, Large-sized few-layer graphene enables an ultrafast and long-life aluminum-ion battery, Adv. Energy Mater. 7 (15) (2017) 1700034.
[9] A.S. Childress, P. Parajuli, J. Zhu, R. Podila, A.M. Rao, A Raman spectroscopic study of graphene cathodes in high-performance aluminum ion batteries, Nanomater. Energy 39 (2017) 69–76.
[10] D.-Y. Wang, C.-Y. Wei, M.-C. Lin, C.-J. Pan, H.-L. Chou, H.-A. Chen, M. Gong, Y. Wu, C. Yuan, M. Angell, Y.-J. Hsieh, Y.-H. Chen, C.-Y. Wen, C.-W. Chen, B.-J. Hwang, C.-C. Chen, H. Dai, Advanced rechargeable aluminium ion battery with a high-quality natural graphite cathode, Nat. Commun. 8 (2017) 14283.
[11] H. Chen, F. Guo, Y. Liu, T. Huang, B. Zheng, N. Ananth, Z. Xu, W. Gao, C. Gao, A defect-free principle for advanced graphene cathode of aluminum-ion battery, Adv. Mater. 29 (12) (2017) 1605958.
[12] K.V. Kravchyk, S. Wang, L. Piveteau, M.V. Kovalenko, Efficient aluminum chloride–natural graphite battery, Chem. Mater. 29 (10) (2017) 4484–4492.
[13] J.S. Wilkes, J.A. Levisky, R.A. Wilson, C.L. Hussey, Dialkylimidazolium chloroaluminate melts: a new class of room-temperature ionic liquids for electrochemistry, spectroscopy and synthesis, Inorg. Chem. 21 (3) (1982) 1263–1264.
[14] J.J. Lee, I.T. Bae, D.A. Scherson, B. Miller, K.A. Wheeler, Underpotential deposition of aluminum and alloy formation on polycrystalline gold electrodes

from AlCl3/EMIC room-temperature molten salts, J. Electrochem. Soc. 147 (2) (2000) 562–566.
[15] T. Jiang, M.C. Brym, G. Dubé, A. Lasia, G. Brisard, Electrodeposition of aluminium from ionic liquids: Part I—electrodeposition and surface morphology of aluminium from aluminium chloride (AlCl 3)–1-ethyl-3-methylimidazolium chloride ([EMIm] Cl) ionic liquids, Surf. Coating. Technol. 201 (1) (2006) 1–9.
[16] S.-J. Pan, W.-T. Tsai, J.-K. Chang, I.-W. Sun, Co-deposition of Al–Zn on AZ91D magnesium alloy in AlCl 3–1-ethyl-3-methylimidazolium chloride ionic liquid, Electrochim. Acta 55 (6) (2010) 2158–2162.
[17] M. Zhang, X. Song, X. Ou, Y. Tang, Rechargeable batteries based on anion intercalation graphite cathodes, Energy Storage Mater 16 (2018) 65–84.
[18] W. Rüdorff, U. Hofmann, Über graphitsalze, Z. Anorg, Allg. Chem. 238 (1) (1938) 1–50.
[19] N. Daumas, Relations between phase concept and reaction mechanics in graphite insertion compounds, CR Acad. Sci., Ser. C 268 (1969) 373.
[20] J.O. Besenhard, M. Winter, Advances in battery technology: rechargeable magnesium batteries and novel negative-electrode materials for lithium ion batteries, ChemPhysChem 3 (2) (2002) 155–159.
[21] J. Xu, Y. Dou, Z. Wei, J. Ma, Y. Deng, Y. Li, H. Liu, S. Dou, Recent progress in graphite intercalation compounds for rechargeable metal (Li, Na, K, Al)-Ion batteries, Adv. Sci. 4 (10) (2017) 1700146.
[22] S.C. Jung, Y.-J. Kang, D.-J. Yoo, J.W. Choi, Y.-K. Han, Flexible few-layered graphene for the ultrafast rechargeable aluminum-ion battery, J. Phys. Chem. C 120 (25) (2016) 13384–13389.
[23] P. Bhauriyal, A. Mahata, B. Pathak, The staging mechanism of AlCl 4 intercalation in a graphite electrode for an aluminium-ion battery, Phys. Chem. Chem. Phys. 19 (11) (2017) 7980–7989.
[24] D. DiVincenzo, E. Mele, Self-consistent effective-mass theory for intralayer screening in graphite intercalation compounds, Phys. Rev. B 29 (4) (1984) 1685.
[25] M. Dresselhaus, G. Dresselhaus, Intercalation compounds of graphite, Adv. Phys. 30 (2) (1981) 139–326.
[26] X. Qi, B. Blizanac, A. DuPasquier, P. Meister, T. Placke, M. Oljaca, J. Li, M. Winter, Investigation of PF 6– and TFSI– anion intercalation into graphitized carbon blacks and its influence on high voltage lithium ion batteries, Phys. Chem. Chem. Phys. 16 (46) (2014) 25306–25313.
[27] M. Wu, B. Xu, L. Chen, C. Ouyang, Geometry and fast diffusion of AlCl 4 cluster intercalated in graphite, Electrochim. Acta 195 (2016) 158–165.
[28] S. Miyoshi, T. Akbay, T. Kurihara, T. Fukuda, A.T. Staykov, S. Ida, T. Ishihara, Fast diffusivity of PF6–anions in graphitic carbon for a dual-carbon rechargeable battery with superior rate property, J. Phys. Chem. C 120 (40) (2016) 22887–22894.
[29] D. Koningsberger, R. Prins, X-ray Absorption: Principles, Applications, Techniques of EXAFS, SEXAFS, and XANES, X-Ray Absorption: Principles, Applications, Techniques of EXAFS, SEXAFS, and XANES, Wiley & Sons, New York, 1988.
[30] A.E. Russell, A. Rose, X-ray absorption spectroscopy of low temperature fuel cell catalysts, Chem. Rev. 104 (10) (2004) 4613–4636.
[31] Y.-W. Tsai, Y.-Y. Chang, Y.-H. Wu, K.-Y. Lee, S.-L. Liu, S.-L. Chang, High-resolution interference-monochromator for hard X-rays, Optic Express 24 (26) (2016) 30360–30367.
[32] Y.-F. Song, C.-H. Chang, C.-Y. Liu, S.-H. Chang, U.-S. Jeng, Y.-H. Lai, D.-G. Liu, S.-C. Chung, K.-L. Tsang, G.-C. Yin, J.-F. Lee, H.-S. Sheu, M.-T. Tang, C.-S. Hwang, Y.-K. Hwu, K.S. Liang, X-ray beamlines for structural studies at the NSRRC superconducting wavelength shifter, J. Synchrotron Radiat. 14 (4) (2007) 320–325.
[33] U.-S. Jeng, C.H. Su, C.-J. Su, K.-F. Liao, W.-T. Chuang, Y.-H. Lai, J.-W. Chang, Y.-J. Chen, Y.-S. Huang, M.-T. Lee, K.-L. Yu, J.-M. Lin, D.-G. Liu, C.-F. Chang, C.-Y. Liu, C.-H. Chang, K.S. Liang, A small/wide-angle X-ray scattering instrument for structural characterization of air-liquid interfaces, thin films and bulk specimens, J. Appl. Crystallogr. 43 (1) (2010) 110–121.
[34] S.J. Clark, M.D. Segall, C.J. Pickard, P.J. Hasnip, M.I. Probert, K. Refson, M.C. Payne, First principles methods using CASTEP, Z. für Kristallogr. - Cryst. Mater. 220 (5/6) (2005) 567–570.
[35] S.-P. Gao, C.J. Pickard, A. Perlov, V. Milman, Core-level spectroscopy calculation and the plane wave pseudopotential method, J. Phys. Condens. Matter 21 (10) (2009) 104203.
[36] J.P. Perdew, K. Burke, M. Ernzerhof, Generalized gradient approximation made simple, Phys. Rev. Lett. 77 (18) (1996) 3865.
[37] H. Chen, H. Xu, S. Wang, T. Huang, J. Xi, S. Cai, F. Guo, Z. Xu, W. Gao, C. Gao, Ultrafast all-climate aluminum-graphene battery with quarter-million cycle life, Sci. Adv. 3 (12) (2017) eaao7233.
[38] G. Schmuelling, T. Placke, R. Kloepsch, O. Fromm, H.-W. Meyer, S. Passerini, M. Winter, X-ray diffraction studies of the electrochemical intercalation of bis (trifluoromethanesulfonyl) imide anions into graphite for dual-ion cells, J. Power Sources 239 (2013) 563–571.
[39] X. Zhang, N. Sukpirom, M.M. Lerner, Graphite intercalation of bis (trifluoromethanesulfonyl) imide and other anions with perfluoroalkanesulfonyl substituents, Bull. Mater. Sci. 34 (3) (1999) 363–372.
[40] H.-J. Liao, Y.-M. Chen, Y.-T. Kao, J.-Y. An, Y.-H. Lai, D.-Y. Wang, Freestanding cathode electrode design for high-performance sodium dual-ion battery, J. Phys. Chem. C 121 (44) (2017) 24463–24469.
[41] B. Özmen-Monkul, M.M. Lerner, The first graphite intercalation compounds containing tris (pentafluoroethyl) trifluorophosphate, Carbon 48 (11) (2010) 3205–3210.
[42] M.S. Dresselhaus, G. Dresselhaus, Intercalation compounds of graphite, Adv. Phys. 51 (1) (2002) 1–186.
[43] A.B. Altman, C. Pemmaraju, C.m. Camp, J. Arnold, S.G. Minasian, D. Prendergast, D.K. Shuh, T. Tyliszczak, Theory and X-ray absorption spectroscopy for aluminum coordination complexes—Al K-edge studies of charge and bonding in (BDI) Al,(BDI) AlR2, and (BDI) AlX2 complexes, J. Am. Chem. Soc. 137 (32) (2015) 10304–10316.
[44] Y.-S. Lin, H.-R. Lin, W.-L. Liu, Y.T. Lee, C.-M. Tseng, C.-K. Ni, C.-L. Liu, C.-C. Tsai, J.-L. Chen, W.-P. Hu, Measurement and prediction of the NEXAFS spectra of pyrimidine and purine and the dissociation following the core excitation, Chem. Phys. Lett. 636 (2015) 146–153.